R. & M. No. 3572

MINISTRY OF TECHNOLOGY

AERONAUTICAL RESEARCH COUNCIL
REPORTS AND MEMORANDA

The Subcritical Response and Flutter of a Slender Wing Model Aircraft

By D. B. PAYEN and P. R. GUYETT
Structures Dept. R.A.E. Farnborough

LONDON: HER MAJESTY'S STATIONERY OFFICE
1969
PRICE 15*s.* 6*d.* NET

The Subcritical Response and Flutter of a Slender Wing Model Aircraft

By D. B. PAYEN and P. R. GUYETT
Structures Dept. R.A.E. Farnborough

Reports and Memoranda No. 3572*
September, 1967

Summary.

An aeroelastic model aircraft of slender planform has been tested in a wind tunnel at low subsonic speeds. The tests comprised measurement of the resonant frequencies and dampings of the first five symmetric modes of deformation with the model mounted on a novel low-stiffness support at mean angles of incidences of $+15°$, $+5°$, $0°$, $-5°$, $-15°$. For zero incidence the speed range was extended to include measurements at speeds up to the critical flutter speed. The results were compared with calculated values based on the five measured still air modes and rigid body motions of the model on its support. Good agreement was obtained for the response in the model deformation modes 1, 2, 3 and 5, and the flutter speed and frequency were predicted accurately. In the mode which became unstable, however, the calculated damping values were somewhat lower than the measured values at subcritical wind speeds.

LIST OF CONTENTS

*Replaces R.A.E. Tech. Report No. 67 225 (A.R.C. 29 916).

---

1. *Introduction.*

The adoption of the slender wing for supersonic transport aircraft has posed a number of questions for the aeroelastician. One of the fundamental questions is whether the theoretical methods that have proved adequate in the past for predicting flutter will be reliable for the new planform. There are several reasons for doubt. On the aerodynamic side it has not previously been necessary to take into account a large amount of chordwise deformation of a wing in the lower modes of oscillation. Moreover, in contrast to earlier aircraft, there is significant variation in the air flow pattern over a slender wing with incidence involving the formation of a vortex system at the leading edge. The effect of these features on the flutter characteristics of a slender wing model are studied in the present Report.

The experiment involved the determination of the dampings and frequencies of the natural modes of oscillation of a flexible model scaled for testing at low subsonic speeds. Investigation of these characteristics at speeds below the critical or flutter speed is referred to as subcritical response measurement.

A novel form of construction was adopted for the model, which was influenced by two main considerations. For practicable applications the stiffness of models for testing in low-speed flow is low, and difficult to achieve in a structural arrangement that attempts to follow the stressed skin design of modern high-speed aircraft. In addition the chordwise flexibility of low aspect ratio wings cannot be represented adequately by the more conventional single-spar or torsion-box type of model construction[1]. In the present arrangement the stiffness and mass distribution requirements were satisfied by building a plane network of interconnected metal beams with weights attached, which formed the skeleton of the model. Around the skeleton a flexible polyurethane foam plastic was cast to provide the desired aerodynamic profile.

Throughout the experiment the model was mounted on a specially built low-stiffness support rig, which provided rigid body freedoms in heave and pitch. The rig was of novel design and enabled an operator to maintain the model in a preset position against aerodynamic lift forces while providing very flexible support in the vertical plane.

The wind-tunnel tests comprised subcritical response measurements for the first five symmetric modes of the model supported at angles of incidence of $+15°$, $+5°$, $0°$, $-5°$, $-15°$. At zero incidence the measurements were made at speeds up to the critical flutter speed of 218 ft/sec (66·5 m/s), this speed being established by experiment.

At zero incidence subcritical response and flutter calculations were made based on five measured still air modes and the heave and pitch rigid body motions of the model on its support. The flutter condition was accurately predicted both with respect to air speed and frequency and good agreement was obtained with the subcritical response measurements for deformation modes 1, 2, 3 and 5. In the flutter mode however, the calculated damping values were low for air speeds above 100 ft/sec (30·5 m/s).

A full description of an experimental technique similar to that used for determining the dynamic properties of the present model has been given by Irwin and Guyett[2] and is not repeated in this present Report. Based on the work of Kennedy and Pancu[3], Broadbent and Hartley[4] and others, it consists of plotting the locus of the end of the displacement vector, representing the response of the structure to a sinusoidal excitation, as it varies with frequency in the neighbourhood of a resonance. For certain conditions the curve approximates to the arc of a circle and can be analysed to obtain the frequency of the natural mode excited, its decay rate and—from a number of measurements of displacement—its shape.

2. *Apparatus.*

2.1. *Wind Tunnel.*

The tests were made in the R.A.E. 4 ft × 3 ft low-turbulence wind tunnel.

2.2. *Model.*

The model was based upon a projected design for a supersonic transport aircraft. It consisted of a slender wing and fuselage; the control surfaces, engine nacelles and fin of the aircraft not being included. The fuselage projected ahead of the wing, and was circular in section over the region of the nose; the wing was positioned close to the top of the fuselage. In planform the wing was a modified slender delta, the leading edge being rounded at the rear to form the streamwise tips. The straight portion of the leading edge was swept back at an angle of 67°. The semi-span of the wing was 8·63 inches (0·219 m) and its aspect ratio based on the mean geometric chord was 0·6. Its centreline chord (defined by producing the leading edge to the centre of the fuselage) was 25·6 inches (0·65 m), and the maximum thickness to chord ratio on the centreline was 0·035. The leading edges were rounded to a radius of 0·125 inch (0·0032 m) to delay separation of the flow at low angles of incidence. The total length of the model was 34 inches (0·86 m). Table 1 gives the planform co-ordinates.

As a basis for the design of the structure of the model, stiffness and mass scaling factors were chosen so that the following similarity parameters were the same for the model at a wind speed of 100 ft/sec (30·5 m/s) and sea level density, as for the projected aircraft at 450 knots (232 m/s) eas at 36 000 ft (11 000 m) with full fuel:

$$EI/\rho V^2 L^4 \; ; \qquad m/\rho L^3 \; ;$$

where:

E Young's modulus of the structural material,

I second moment of area,

L characteristic length,

V stream velocity,

m characteristic mass, and

ρ stream density.

The stiffness required was achieved in a plane network of interconnected aluminium alloy beams forming a pattern of bays. Over the main section of the wing the beams were chosen to lie in the spanwise and fore-and-aft directions. Each beam at the common side of two adjoining bays was designed with its bending rigidity (EI) varying linearly from one end to the other. The (EI) at each end was found from estimates of the rigidity of the section of the full scale structure over the region corresponding to the mid-bay position on one side of the beam to the mid-bay position on the other side. Fig. 1a shows the arrangement adopted for the metal framework.

The required mass was realised on the model by attaching weights of GEC Heavy Alloy* to the metal framework.

*GEC Heavy Alloy has a specific gravity of 16·5.

One of the factors considered in designing the metal framework was the need to obtain a structure in which the stiffness over the working range was independent of the deflected shape. With a thin flat plate, pronounced changes in stiffness can occur when the plate deflects out of its plane, but these changes are reduced by removing material from the plate to form a network of beams. Tests were made to investigate this effect on specimens having various configurations and the form of the skeleton used in the model was chosen on the basis of the results. Measurements made on the completed model showed that the non-linearities were not significant.

The metal framework was manufactured from 10 swg duralumin plate using a chemical etching process to provide areas of constant thickness reducing in steps towards the wing tips, and then cutting out the bays on a pantograph-controlled milling machine using templates four times the actual size. Before the machining operation the etched plate was bent downwards at the nose to the required contour of the model and moulded to a wooden block to prevent the slender beams from distorting under the cutting loads. The photographs in Fig. 2 show the plate with one bay cut, the lower half of the mould and the metal framework prior to foaming.

The aerodynamic profile of the model was provided by casting a flexible polyurethane plastic foam around the metal framework. Fingers forming part of the framework extended from the beam intersections towards the centre of the bays. These prevented excessive panting of the foam through the open bays under aerodynamic pressures and helped to transmit the aerodynamic and inertia forces acting on the foam to the metal structure. In addition the fingers provided attachment points for the Heavy Alloy weights.

Fig. 1b shows the completed model. Small diameter screwed rod and perspex filler pieces were used to enable direct attachment to be made to the metal framework at beam intersections. In the photograph these show up as faint dots and black spots on the nose and wing surface of the model.

A difficulty with foam-covered models is that, even though the effective elastic modulus of the foam is extremely small compared to that of the metal, its contribution to static stiffness was in the order of 12 per cent*. This addition was probably caused by large stresses arising in the foam due to its interaction with the support fingers in the metal framework.

It has been shown[5] that the stiffness and damping properties of the plastic foam are dependent on the absolute humidity and temperature of the surrounding air and that the dynamic stiffness is greater than the static value. Maximum recorded changes in frequency and damping of the modes of vibration of the model were in the order of 3 per cent and 20 per cent respectively. Variations of the measured experimental values obtained in the wind-tunnel tests were small, however, as changes in atmospheric condition in the working section were negligible during the test period.

2.3. *Model Support Rig.*

A novel support system allowed the model freedom of movement in heave and pitch while providing restraint in the other overall body motions. The model was mounted in the horizontal plane on two legs. Each leg comprised a support tube which moved on parallel linkages, a low-stiffness spring device and a manual control for varying the reactive load in the support. Attachment of the model to the support tubes was made through nylon bearings fixed to the metal framework on its centreline and positioned 15 inches (0·381 m) apart with the rear bearing 5·3 inches (0·135 m) from the trailing edge of the wing. The forward tube, designed to withstand aerodynamic drag loads, passed vertically through the model and was connected to the hinge linkages above and below it. To allow the model to pitch and bend freely the rear tube was additionally hinged in the fore-and-aft vertical plane. Quick-acting clamps were provided to arrest the motion of the tubes in the event of an aerodynamic instability. A photograph of the rig is given in Fig. 3.

The forward leg is shown in a diagramatic form in Fig. 5. The means by which the low-stiffness was achieved was based on the principle originated by Molyneux[6]. This consists essentially of counteracting a positive stiffness with a negative stiffness. In the present system the negative stiffness was supplied by a

*The contribution of the foam to the stiffness of this type of model depends upon the detailed design of the metal framework and the density of the foam. The average density of the foam in the present model was 11 lb/ft^3 (176 Kg/m^3).

toggle mechanism. This comprised a pair of wires, each tensioned by a spring which exerted a compressive load on two links that were hinged at one end to the support tube and at the other to the main frame of the rig. In the datum position the links were parallel to the tension wires and the resultant force from the toggle on the tube was zero. Any excursion from the datum caused the toggle to exert a vertical force on the support in the direction of displacement with the characteristic of a negative stiffness. The positive balancing stiffness was provided by two coil springs mounted along the axis of the tubes. The arrangement was such that the overall support stiffness increased gradually with displacement from the datum, the change being very small at displacements less than half an inch (0·013 m).

A feature of the system is that the low-stiffness characteristic can be maintained independently of the load acting on the model by adjusting the earthed end of one of the vertical springs to keep the support in the datum position. In each leg of the rig the adjustment was made through a worm drive controlled with a manually-operated lever.

Two further adjustments were provided. Firstly, the mean incidence of the model could be set by varying the length of the front support tube between the model and the spring suspension system. Secondly, the overall stiffness of each support leg could be varied by altering the working length of the lower coil spring.

Although it was possible to achieve zero stiffness at the datum position, this condition proved extremely sensitive to changes in the length of the vertical spring. The aim was therefore to work with a low stiffness rather than a zero stiffness. During the tests in the wind tunnel it was found necessary to increase the stiffness of the rear support to avoid a rigid-body instability of the model. The final stiffnesses were 0·50 lb/in (88·0 N/m) for the front leg and 1·65 lb/in (290 N/m) for the rear. A curve showing the variation of deflection with load for the front leg is given in Fig. 6.

2.4. *Excitation.*

Specially-built, electro-dynamic exciters were used to apply oscillatory forcing to the model. Each exciter consisted of a coil placed in a magnetic field which was produced by a permanent magnet. The coil was attached to the support tube and was rectangular in cross-section. This shape was necessary to allow free movement of the coil relative to the magnet as the support legs moved on an arc with the parallel linkages. The arrangement is illustrated in Fig. 5*. The exciters provided an excitation force through a maximum amplitude of half an inch (0·013 m) while allowing a total vertical movement of the support leg of $2\frac{1}{2}$ inches (0·064 m).

Driving current in the coils was obtained by amplifying the signal from a decade oscillator. The current was monitored using a resistor connected in series with the coil.

2.5. *Instrumentation.*

A block diagram of the instrumentation showing the function of each item is given in Fig. 7.

Electrical signals proportional to the displacement of the model were obtained in two ways. In the measurements of the resonant modes of the model in still air the signal was obtained from a vibration meter. This instrument detected changes in capacitance between a metal surface and a probe. Details of the procedure used are given in Section 3.1. In the wind tunnel the signal was obtained from sets of strain gauges attached to the metal framework within the model. Each set of gauges comprised two pairs placed symmetrically about the centreline of the fuselage, the individual gauges in a pair being stuck to the top and bottom surfaces of the structure at the one location. This enabled the four gauges to be connected externally into a Wheatstone bridge sensitive to symmetric deformation of the model and unresponsive to anti-symmetric deformations or *vice versa.*

In both cases the response signal was resolved into components in-phase and in-quadrature with a reference signal produced by the oscillator controlling the exciter drive. Direct current voltages propor-

*The exciters were offset from the support tubes because a mechanical exciter (not used in the present experiment) occupied the space immediately below the lower spring on each support leg.

tional to the components were supplied to an X-Y plotter.

The accuracy with which it was possible to determine the response was dependent upon the steadiness of the signals. However, for the comparative measurements of amplitudes in still air the accuracy was about ± 2 per cent of full scale deflection of the co-ordinates of the X-Y plotter.

3. *Measurement of Modes in Still Air.*

3.1. *Test Procedure.*

For the purposes of defining the mode shapes and mass distribution of the model, the planform was divided into 50 regions having mass centres at or close to beam intersection points on the metal framework, these points being convenient stations at which to measure model displacement. The boundaries of these regions are shown in Fig. 8 while the co-ordinates of the mass centres are given in Table 2. The measuring stations on the centreline and port wing of the model were numbered 1 to 32, the remaining eighteen being symmetrically placed on the starboard wing. At each station it was necessary to provide a metal surface for use in conjunction with the displacement measuring probe. These consisted of light-weight discs of balsa and tinfoil fixed to duralumin stems which were attached directly to the metal framework. The probes were held in position close to the face of the discs by mounting them in a wooden board fixed above the model. With the model mounted at zero incidence on its support and excitation rig, a vector response plot was obtained at each of the measuring stations for each of the modes measured. The procedure used throughout the investigation of a particular mode was as follows:

Single point excitation was adopted and, of the two exciter positions, that best suited to excite the mode was chosen. The force input to the model was kept constant by monitoring and adjusting, when necessary, the current flowing in the coil. The excitation frequency was varied in equal steps through the resonant condition. At each frequency a point was obtained on the X-Y plotter graph defining the response vector.

Displacement response was measured in the first five deformation modes and two rigid body modes of the model on its support.

3.2. *Determination of Mode Shapes and Orthogonality Check.*

Typical response plots obtained in the above tests are displayed in Fig. 9. In nearly all cases the curves were arcs of circles over the portion passing through the resonant frequency of the mode, thus enabling the required circle to be constructed. The centre of the circle however, very rarely coincided with the quadrature co-ordinate axis of the plot, as it would in a single-degree-of-freedom case. This indicated that the forcing applied to the model was not able to excite the individual pure normal modes of the system. In these circumstances the mode shapes were determined by assuming that the displacement in the normal mode at a measuring station was proportional to the diameter of the constructed circle*. The resonant frequency and damping of each mode was found by averaging the values obtained from a number of the best plots in each set. The frequency was assumed to be indicated by a point on the circles where the change of frequency with arc length was a minimum. Direct damping values were deduced from the relationship:

$$\frac{C}{C_c} = \frac{\omega_A - \omega_B}{2\omega_R} \times \operatorname{Cot} \theta/2 ,$$

ω_R is the chosen resonant frequency of the mode and ω_A and ω_B are two adjacent frequencies such that $\omega_B < \omega_R < \omega_A$. These frequencies represent points on the circle such that the arcs ω_A to ω_R and ω_R to ω_B subtend equal angles θ at the centre of curvature. The quantity C/C_c is the ratio of the actual or equivalent (in the case of hysteretic damping) velocity damping in the system to the critical damping required to

*In Ref. 2 an assessment was made of three ways of deducing normal modes from vector response plots. The results suggest that the method used in the present investigation gives the best approximation to the required normal modes.

change the free motion of the system from periodic to aperiodic. This approach, which is discussed in greater detail in Ref. 2, is based on the assumption that the parts of the vector response curves through which circles are constructed may be treated as the response of a system with a single-degree-of-freedom.

Figs. 9 to 13 show the shapes of the model deformation modes and Table 3 gives the non-dimensional displacements at each measuring station for these and the rigid-body modes, any small asymmetric discrepancies having been averaged out.

One way of assessing the accuracy of the measured modes is to examine the magnitude of their cross inertias. To do this requires a knowledge of the mass distribution of the model. The mass associated with each measuring station was found by estimation and measurement (*see* Section 6.1.2). The resulting mass distributions may be seen in Table 4. Having established the mass and mode displacement at each measuring station a matrix of generalised inertia coefficients was obtained. The assessment of cross inertia magnitudes was facilitated by dividing the matrix elements a_{RS} by $\sqrt{a_{RR}\, a_{SS}}$ where the suffices R and S refer to modes R and S respectively. The resultant non-dimensional coefficients are given in Table 6.

Based on a generally acceptable level of 10 per cent for the cross inertias of measured modes, the orthogonality check is considered to be satisfactory. The only cross inertias above this figure are those between Modes 1 and 2 (16 per cent) and Modes 2 and 3 (11 per cent); where model deformation modes are concerned the next largest is 5·6 per cent. Modes 1 and 2 are fairly likely in shape and the cross inertia between them is very sensitive to small changes in the shape of the second mode. The 11 per cent cross inertia is probably due to close proximity of the frequencies of Modes 2 and 3 and suggests that the method of analysis was not able to separate completely the pure modes, each identified mode being a combination of the two orthogonal modes. Overall evidence, however, indicates that the deduced mode shapes are close to the normal modes of the system.

It has been pointed out in Section 2.2 that there was some variation in the dynamic characteristics of the model with changes in atmospheric conditions. In view of this the still-air values of frequency and damping of the modes given in Figs. 10 to 14 and Table 7 were those found during the measurements of subcritical response with the model in the wind tunnel, and therefore apply directly to the subcritical response results and analysis.

4. *Measurement of Subcritical Response.*

4.1. *Test Procedure.*

The model and support rig were installed in the wind tunnel with the support tubes passing through the floor and roof of the working section. Aerodynamic drag loads were reduced by streamlining the parts of the supports near the model with balsa wood and shielding the remaining tube lengths with metal fairings fixed to the tunnel structure. The photograph of Fig. 4 shows the arrangement.

For angles of incidence greater than zero a band of grit Grade 60, about a $\frac{1}{4}$ inch (0·0064 m) wide was glued to the surface of the wing and around the nose to fix the position of transition. In the 15° case the band on the wing was applied along a line from the junction of wing and fuselage to the trailing edge 1 inch (0·025 m) inboard of the tip. For 5° incidence testing this band was positioned parallel to, and $\frac{5}{8}$ inch (0·016 m) inboard of the leading edge. During a test run the rig operator, controlling the position of the model, progressively adjusted the load in the support tube as the aerodynamic lift force varied with wind speed.

Vector plots were obtained of model response to a sustained excitation at wing speeds up to 212 ft/sec (64·6 m/s). The method used was similar to that described in Section 3.1, the difference being that strain gauges were used to monitor model displacement. One mode was investigated in a test run covering in steps the required range of air speed. This procedure was followed for the first five deformation modes with the model at zero incidence, and for the first four modes at $-15°$, $-5°$, $+5°$ and $+15°$ incidence. The maximum airspeeds at 5° and 15° incidence were limited to 120 ft/sec (36·6 m/s) and 80 ft/sec (24·4 m/s) respectively by the total amount of adjustment available in the support rig for counteracting model lift forces.

During early runs at zero incidence a rigid body instability of the model on its support developed at wind speeds above 80 ft/sec (24·4 m/s). This took the form of a galloping motion in pitch and heave which

grew rapidly in amplitude. The instability was cured by increasing the stiffness of the rear support.

4.2. *Test Results.*

Apart from a few plots obtained at the top end of the speed range, the vector response curves were free from significant scatter or distortion and could be analysed readily to obtain the resonant frequencies and damping values for the system. The scatter in two of the worst plots can be seen in Fig. 8f and 8g. This was due to random movements of the model which increased at speeds approaching flutter.

Resonant frequencies were found from the response plots for each test condition in the same way as in still air, namely from estimates of the position on the response curves at which the indicated change of frequency with arc length was a minimum. When the damping was low the coefficient of damping was calculated by the method described in Section 3.2. When the damping was high, however, an alternative procedure was used due to Woodcock[7]. The natural frequency of the free motion of the system was found from the relationship:

$$\omega_R^2 = \mu^2 + \nu^2$$

where ω_R is the chosen resonant frequency,

μ is the exponential rate of decay, and

ν is the natural frequency of the motion.

Figs. 15 to 18 show the variation of the frequency of free motion and damping with wind speed for the first five modes of the model at zero incidence. Damping values at the other angles of incidence are plotted against wind speed in Figs. 19 to 20 and the resonant frequencies are given in Table 8. The results are discussed in Section 7.

5. *Flutter Tests.*

Subcritical response measurements were made at increasing wind speeds and the vector plots analysed immediately to indicate the variation in damping of the modes. When the damping in the fourth mode began to fall, smaller increments were taken in wind speed until the flutter speed and frequency could be predicted with some certainty. At this stage the excitation frequency was set to the predicted value and the force input to the model reduced. The wind speed was then increased in very small steps until a speed was reached at which the amplitude of oscillation began to build up. The excitation was switched off at the onset of instability and a record of the motion obtained by means of an ultra-violet recorder to give the flutter frequency. Subsequently the motion was stabilised by reducing the wind speed. Repeat measurements gave flutter speeds in the range 217–219 ft/sec (66·1–66·8 m/s).

6. *Calculation of the Subcritical Response and the Flutter Condition.*

The equations of motion of the system were derived by applying Lagrange's equations. The degrees of freedom chosen and the preparation of the coefficients is described in Section 7.1. A digital computer was used to obtain the roots of the equations of free motion in the way outlined in Section 7.2.

6.1. *Preparation of the Coefficients.*

6.1.1. *Mode shapes.* The shapes of the first five model modes and the two rigid-body modes of the model on its support, deduced from the measurements of response in still air, were taken as the degrees of freedom of the system. Those modes are given in Figs. 10 to 14 and Table 3.

6.1.2. *Structural inertia.* The mass of each of the regions into which the model was divided (*see* Fig. 8) was found from direct measurement and estimations of the weight of duralumin, heavy metal, plastic foam and other components in the region. Items such as added masses were weighed before

assembly to the model and the density of the foam (assumed to be uniform) was found from a knowledge of its total weight and volume. An indication of the accuracy of the estimated distribution of mass is given from the fact that the total weight of the metal plate, based on estimates of its volume and density, agreed to within 2 per cent of the actual measured weight, and the estimated volume of the model agreed to within 4 per cent of the measured volume of the former from which it was cast. Finally the effective mass of each support leg was found separately, with the model disconnected, by determining the variation of the support resonant frequency with the addition of small masses. The mass distribution may be seen in Table 4.

The generalised inertias in the chosen degrees of freedom were subsequently found from the mass data and mode shapes, and are given in Table 5.

6.1.3. *Structural stiffness.* For each degree of freedom the direct stiffness term was deduced from the direct generalised inertia and the mode frequency as measured in still air in the wind tunnel. The majority of the results presented in this Report were found assuming zero cross-stiffness terms. Some calculations were made, however, using approximate cross stiffnesses estimated from the geometric mean of the still air frequencies of the modes considered and the generalised cross inertia between them. Mode frequencies are listed in Table 7.

6.1.4. *Structural damping.* The direct damping values for each mode were found from the results of the response measurements in still air. These values were converted into the equivalent viscous damping form to suit the digital calculation procedure. Table 7 lists the coefficients. All structural cross-damping coefficients were assumed to be zero.

6.1.5. *Oscillatory aerodynamic forces.* Oscillatory aerodynamic-force coefficients were found by means of the Mercury Digital Computer Programme R.A.E. 161A prepared by D. E. Davies. This programme gives the generalised aerodynamic coefficients for a wing oscillating harmonically in rigid or flexible modes at subsonic speeds. In making the calculation, eight displacement and upwash points were taken along the chord line at each of five spanwise stations on the half wing. The programme requires as data the displacement and slope in the modes at each of these collocation points. This information was obtained conveniently by finding a polynomial expression in X and Y of order 6 to represent each mode. Mercury Digital Computer Programme R.A.E. 194/A prepared by J. H. Cadwell was used to obtain the polynomial coefficients.

Values of the aerodynamic forces were determined for a number of frequency parameters*.

6.2. *Calculation of the Free Motion of the Model.*

The roots of the equations of motion were found using the Mercury Digital Computer Programme R.A.E. 272/A written by LL. T. Niblett. The roots describe the rate of decay (or growth) and frequency of the free motion of the natural modes at a particular wind speed for a set of aerodynamic force coefficients appropriate to a particular frequency parameter. Since frequency parameter is a function of both wind speed and frequency, the calculated values of rates of decay and frequency for a particular mode at a given wind speed should be obtained using aerodynamic coefficients for a frequency parameter based on that wind speed and the calculated frequency of the mode. In the present case, however, no effort was made to match the frequency parameters exactly at each speed because the answers were not very sensitive to variation of frequency parameter. In fact the maximum error involved in using a constant frequency parameter throughout, based on the critical flutter speed and frequency, was approximately 8 per cent of the damping values in the first mode and under 4 per cent in the remaining modes; the variation in the frequencies was smaller.

*Frequency parameter is defined as

$$\frac{\text{(angular frequency of oscillation)} \times \text{(wing mean chord)}}{\text{wind speed}}$$

Further calculations were made at a single frequency parameter based on the flutter condition, as follows:

(i) Cross inertia and structural stiffness terms were included separately and together.

(ii) The rigid-body degrees-of-freedom were omitted.

(iii) Structural damping values were treated as being of a hysteretic rather than viscous nature.

(iv) All structural damping coefficients were set to zero.

(v) The degrees-of-freedom of modes 1, 2, 3 and 5 were omitted separately in turn.

(vi) Two binary and one ternary calculations were made based on modes 2 and 4, modes 3 and 4, and modes 2, 3 and 4 respectively.

The effect of (i), (ii) and (iii) on the calculated response was very small, but the results obtained from (iv), (v) and (vi) gave some insight into the characteristics and mechanism of the flutter. These results are shown in Fig. 21 and discussed in Section 7.3.

7. *Comparison and Discussion of Measured and Calculated Results.*

7.1. *Subcritical Response at Zero Incidence.*

The measured frequencies and rates of decay of the first five natural modes of deformation of the model are shown in Figs. 15 to 18, together with values obtained from the main series of calculations described in Section 6.2. There is some scatter of the experimental results, but the agreement in the general levels and trends of the curves is good. From Fig. 15 it is clear that the frequencies of the modes remained well separated at all speeds. The biggest discrepancy between the theoretical and experimental damping results was in the fourth mode at subcritical speeds. One of the consequences of this discrepancy is that the rate of change of damping with wind speed at the approach to flutter is greater in the experimental result than in the theoretical prediction.

The reasons for this disagreement are not clear. It is unlikely that inaccuracies in the representation of the inertia and stiffness are the cause as the calculations, which excluded cross inertias and included approximate values of cross stiffness and damping, showed little change in the values of the calculated roots. Explanations based on aerodynamic interference from the wind-tunnel walls or model supports are difficult to support for two reasons: firstly it appears[8,9] that wall interference in a closed tunnel is small for the size of model used in this experiment; and secondly, the agreement of response is good in the other modes. One source of error in the theoretical aerodynamic forces is that the influence of the fuselage was neglected.

7.2. *The flutter condition.*

Agreement between the calculated and measured flutter condition at zero incidence was good. The average flutter speed and frequency was 218 ft/sec (66·5 m/s) and 38·4 cycles/sec respectively, against the calculated values of 218·6 ft/sec (66·6 m/s) and 39·0 cycles/sec.

7.3. *Effect of Angle of Incidence on the Subcritical Response.*

The variation of dynamic response of the model with angle of incidence may be assessed from Figs. 19 to 20 and Table 8. It should be noted that at $\pm 5°$ incidence, examination showed that separated air flow with a leading edge vortex was not fully established over the surface of the wing. Separated flow had developed completely however, at angles greater than 10°.

Within the range of wind speed considered, the results show generally that the effect of incidence was small, particularly on frequency. There are indications however, that the rates of decay increase more rapidly with wind speed at the larger angles of incidence. This is especially evident in mode 3. It also appears that a considerable degree of symmetry exists between results obtained at positive and negative angles of incidence of the same magnitude.

7.4. *Observations on the Flutter Characteristics of the Model.*

From the results of the calculations in which certain of the modes of deformation were omitted it is possible to make some observations about the flutter characteristics of the model. These results are presented in Fig. 21. Omitting modes 1 and 5 had very little influence, but when modes 2 or 3 were left out the predicted flutter speed increased substantially, the omission of mode 2 having by far the greater effect. In view of this result the calculations specified in 6.2 (vi) were made which showed that a very close approximation to the flutter speed could be obtained using modes 2, 3 and 4 alone. The binary in modes 2 and 4 gave a better prediction than that in modes 3 and 4. This is an interesting result since it is apparent that the reduction in damping in mode 4 is accompanied by a rapid increase in damping of mode 3, thus giving the impression that modes 3 and 4 are dominant in the flutter.

Another curve in Fig. 21 shows the effect of reducing the structural damping in the degrees-of-freedom to zero. The flutter speed is reduced from 218 ft/sec (66·5 m/s) to 170 ft/sec (51·8 m/s), indicating the significance of structural damping in the system.

8. *Conclusions.*

An investigation has been made into the flutter and subcritical response of an aero-elastic model of slender planform. The resonant frequencies and dampings of the first five symmetric modes of the model were measured at wind speeds up to the critical flutter speed of 218 ft/sec (66·5 m/s), with the model mounted at zero incidence on a special low-stiffness support. Similar measurements were also made with the model at incidences of $+15°$, $+5°$, $-5°$ and $-15°$, up to a wind speed of 120 ft/sec (36·6 m/s).

The technique employed consisted of the direct measurement of the displacement vector response of the model to a sustained excitation. Curves giving the vector response with frequency were analysed by the methods given in Ref. 2.

For the zero incidence case the results are generally in good agreement with the results of calculations in seven degrees of freedom, these comprising the first five modes of deformation measured in still air and the rigid body motions of the model on its support; the flutter speed and frequency was predicted almost exactly. Further theoretical investigations show that a close approximation to the calculated behaviour could be obtained using three of the modes of deformation only, as degrees of freedom. The experimental results at positive and negative incidence indicate that the associated change in flow had little effect upon the frequencies and rates of decay of the modes.

The model was of novel construction and consisted of a framework of metal beams moulded within a block of flexible polyurethane foam plastic of the required profile. This modelling technique, developed for aero-elastic models to be tested at low subsonic speeds, appears to provide a satisfactory means of representing the chordwise flexibilities of slender-wings.

REFERENCES

No.	Author(s)	Title, etc.
1	W. G. Molyneux	Aeroelastic modelling. R.A.E. Technical Note Structures 353 (1964). A.R.C. 25865,
2	C. A. K. Irwin and P. R. Guyett	The subcritical response and flutter of a swept-wing model. A.R.C. R. & M. 3497 (1965).
3	C. C. Kennedy and C. D. P. Pancu	Use of vectors in vibration measurement and analysis. *J. Aero. Sci.* 14, 11, 603–625 (1947).
4	E. G. Broadbent and E. V. Hartley	Vectorial analysis of flight flutter test results. A.R.C. R. & M. 3125 (1958).
5	D. B. Payen	Stiffness, damping and creep properties of a polyurethane foam including the effects of temperature and humidity. A.R.C. C.P. 905 (1967).
6	W. G. Molyneux	The design of flexible supports for vibration isolation. R.A.E. Technical Note Structures 277. (1960). A.R.C. 22212.
7	D. L. Woodcock	On the interpretation of the vector plots of forced vibrations of a linear system with viscous damping. *Aeronaut. Quart.* 14, 1, 45–62 (1963).
8	W. E. A. Acum	A note on the estimation of the effect of wind tunnel walls on the forces on slowly oscillating slender wings. A.R.C. C.P. 707 (1963).
9	W. G. Molyneux	Wind tunnel interference in dynamic measurements. R.A.E. Technical Report 64069, A.R.C. 26673 (1964).

TABLE 1

Co-Ordinates of the Planform of Model

X co-ordinate measured from nose		*Y* co-ordinate measured from centre line		*X* co-ordinate measured from nose		*Y* co-ordinate measured from centre line	
in	cm	in	cm	in	cm	in	cm
1	2·54	0·52	1·32	18	45·72	3·73	9·47
2	5·08	0·65	1·65	19	48·26	4·16	10·57
3	7·62	0·77	1·96	20	50·80	4·58	11·63
4	10·16	0·88	2·24	21	53·34	5·00	12·70
5	12·70	0·98	2·49	22	55·88	5·42	13·77
6	15·24	1·04	2·64	23	58·42	5·84	14·83
7	17·78	1·09	2·77	24	60·96	6·22	15·80
8	20·32	1·15	2·92	25	63·50	6·60	16·76
9	22·86	1·20	3·05	26	66·04	6·97	17·70
10	25·40	1·25	3·18	27	68·58	7·32	18·59
11	27·94	1·27	3·23	28	71·12	7·63	19·38
12	30·48	1·30	3·30	29	73·66	7·92	20·12
13	33·02	1·60	4·06	30	76·20	8·16	20·73
14	35·56	1·98	5·03	31	78·74	8·33	21·16
15	38·10	2·42	6·15	32	81·28	8·50	21·59
16	40·64	2·85	7·24	33	83·82	8·58	21·79
17	43·18	3·28	8·33	34	86·36	8·63	21·92

TABLE 2

Co-Ordinates of the Measuring Stations on Model

Model station	*X* co-ordinate measured from nose		*Y* co-ordinate measured from centre line		Model station	*X* co-ordinate measured from nose		*Y* co-ordinate measured from centre line	
	in	cm	in	cm		in	cm	in	cm
1	1·2	3·05	0	0	17	23·7	60·20	3·25	8·25
2	3·7	9·40	0	0	18	26·2	66·55	3·25	8·25
3	6·2	15·75	0	0	19	28·7	72·90	3·25	8·25
4	8·7	22·10	0	0	20	31·2	79·25	3·25	8·25
5	11·2	28·45	0	0	21	33·7	85·60	3·25	8·25
6	13·7	34·80	0	0	22	18·7	47·50	3·68	9·35
7	16·2	41·15	0	0	23	21·2	53·85	4·71	11·96
8	18·7	47·50	0	0	24	23·7	60·20	5·75	14·61
9	21·2	53·85	0	0	25	26·2	66·55	5·75	14·61
10	23·7	60·20	0	0	26	28·7	72·90	5·75	14·61
11	26·2	66·55	0	0	27	31·2	79·25	5·75	14·61
12	28·7	72·90	0	0	28	33·7	85·60	5·75	14·61
13	31·2	79·25	0	0	29	26·2	66·55	6·68	16·96
14	33·7	85·60	0	0	30	28·7	72·90	7·50	19·05
15	16·2	41·15	2·58	6·55	31	31·2	79·25	8·02	20·38
16	21·2	53·85	3·25	8·25	32	33·7	85·60	8·27	21·01

TABLE 3

Measured Modes

Model station	Normalised displacements						
	Rigid body		Model deformation				
	Heave	Pitch	1st	2nd	3rd	4th	5th
1	1·555	−1·667	1·273	−0·295	0·172	0·186	−0·167
2	1·513	−1·462	0·925	−0·137	0·072	0·018	0·018
3	1·470	−1·257	0·663	−0·052	0·019	−0·064	0·086
4	1·427	−1·051	0·294	0·007	−0·022	−0·084	0·099
5	1·385	−0·846	0·105	0·037	−0·035	−0·054	0·055
6	1·342	−0·641	−0·069	0·044	−0·022	−0·022	0·002
7	1·299	−0·436	−0·163	0·012	0·003	0·043	−0·040
8	1·257	−0·231	−0·295	−0·023	0·033	0·087	−0·068
9	1·214	−0·026	−0·303	−0·060	0·054	0·101	−0·046
10	1·171	0·179	−0·253	−0·084	0·054	0·062	0·006
11	1·128	0·384	−0·100	−0·065	0·023	0·020	0·054
12	1·086	0·589	0·087	−0·003	−0·031	0·007	0·015
13	1·043	0·794	0·332	0·083	−0·088	0·044	−0·133
14	1·000	1·000	0·585	0·184	−0·142	0·102	−0·349
15	1·299	−0·436	−0·302	0·013	0·003	0·049	−0·046
16	1·214	−0·026	−0·430	−0·074	0·064	0·081	−0·071
17	1·171	0·179	−0·326	−0·092	0·066	0·002	−0·019
18	1·128	0·384	−0·156	−0·063	0·049	−0·078	0·025
19	1·086	0·589	0·097	0·034	0·018	−0·086	−0·030
20	1·043	0·794	0·383	0·133	−0·010	−0·006	−0·181
21	1·000	1·000	0·704	0·276	−0·036	0·127	−0·379
22	1·257	−0·240	−0·425	−0·031	0·035	0·090	−0·090
23	1·214	−0·026	−0·372	−0·088	0·075	0·061	−0·091
24	1·171	0·179	−0·329	−0·108	0·107	−0·167	−0·047
25	1·128	0·384	−0·135	−0·065	0·122	−0·318	−0·043
26	1·086	0·589	0·130	0·103	0·144	−0·300	−0·100
27	1·043	0·794	0·402	0·290	0·186	−0·083	−0·135
28	1·000	1·000	0·747	0·523	0·251	0·321	−0·170
29	1·128	0·384	−0·131	−0·072	0·155	−0·442	−0·191
30	1·086	0·589	0·129	0·163	0·240	−0·522	−0·149
31	1·043	0·794	0·486	0·504	0·518	−0·085	0·178
32	1·000	1·000	1·000	1·000	1·000	1·000	1·000

TABLE 4

Mass Distribution of Model

Model station	Mass slug $\times 10^{-3}$	Mass gramme	Model station	Mass slug $\times 10^{-3}$	Mass gramme
1	2·561	36·66	17	7·239	105·73
2	3·530	51·56	18	7·423	108·43
3	3·827	55·90	19	5·912	86·35
4	5·427	79·27	20	2·162	31·58
5	4·774	69·73	21	0·246	3·59
6*	89·186	1302·70	22	0·311	4·54
7	9·446	137·97	23	0·096	1·41
8	16·758	244·77	24	0·299	4·37
9	9·884	144·37	25	3·398	49·63
10	5·736	83·78	26	0·731	10·68
11	17·458	254·99	27	0·780	11·39
12*	95·405	1393·50	28	0·249	3·64
13	6·240	91·14	29	0·097	1·42
14	0·640	9·35	30	0·153	2·24
15	0·087	1·27	31	0·196	2·86
16	4·147	60·57	32	0·096	1·40

*Includes support masses of 81·864 slug $\times 10^{-3}$ or 1195·7 g and 84·908 slug $\times 10^{-3}$ or 1240·2 g at stations 6 and 12 respectively.

Total mass less supports = 0·1713 slug = 2·502 Kg.

TABLE 5

Inertia Matrix for Modes Given in Table: Values given in Slug. $\times 10^{-3}$ *and Gram (in brackets) for Unit Displacement in Modes at Model Station 32*

	Modes						
	Heave (H)	Pitch (P)	1st	2nd	3rd	4th	5th
H	497·26 (7262·9)	−19·887 (−290·48)	−4·6186 (−67·459)	−0·6800 (−9·9321)	1·4737 (21·525)	−2·2164 (−32·373)	−2·3590 (−34·455)
P	−19·887 (−290·48)	123·88 (1809·4)	−1·9412 (−28·353)	0·6142 (8·9707)	−0·1219 (−1·7811)	−0·2835 (−4·1408)	−1·0429 (−15·233)
1st	−4·6186 (−67·459)	−1·9412 (−28·353)	20·314 (296·70)	0·9592 (14·010)	−0·2615 (−3·8200)	0·0564 (0·8235)	0·0369 (0·5384)
2nd	−0·6800 (−9·9321)	0·6142 (8·9707)	0·9592 (14·010)	1·7133 (25·025)	−0·1488 (−2·1731)	−0·0166 (−0·2430)	0·0172 (0·2518)
3rd	1·4737 (21·525)	−0·1219 (−1·7811)	−0·2615 (−3·820)	−0·1488 (−2·7731)	1·0839 (15·831)	0·0156 (0·2279)	0·0120 (0·1753)
4th	−2·2164 (−32·373)	−0·2835 (−4·1408)	0·0564 (0·8235)	−0·0166 (−0·2430)	0·0156 (0·2279)	1·9894 (29·057)	−0·0493 (−0·7195)
5th	−2·3590 (−34·455)	−1·0429 (−15·233)	0·0369 (0·5384)	0·0172 (0·2518)	0·0120 (0·1753)	−0·0493 (−0·7195)	1·1473 (16·758)

TABLE 6

Orthogonality Check on Inertia Matrix

1·000	−0·080	−0·046	−0·023	0·063	−0·070	−0·099
−0·080	1·000	−0·039	0·042	−0·011	−0·018	−0·087
−0·046	−0·039	1·000	0·163	−0·056	0·009	0·008
−0·023	0·042	0·163	1·000	−0·109	−0·009	0·012
0·063	−0·011	−0·056	−0·109	1·000	0·011	0·011
−0·070	−0·018	0·009	−0·009	0·011	1·000	−0·033
−0·099	−0·087	0·008	0·012	0·011	−0·033	1·000

TABLE 7

Model Frequencies and Fractions of Critical Damping in Still-Air

Mode		Frequency *c/s*	Fraction of critical damping C/C_c
Rigid body	Heave	1·45	0·1200
	Pitch	2·90	0·0900
Model deformation	1st	12·1	0·0515
	2nd	22·3	0·0400
	3rd	26·5	0·0300
	4th	42·3	0·0265
	5th	52·0	0·0375

TABLE 8

Comparison of the Variation of Mode Frequency with Wind Speed at Model Incidence Angles of −15°, −5°, 0°, +5°, +15°

Incidence angle		−15°	−5°	0°	+5°	+15°
Wind speed		Freq.	Freq.	Freq.	Freq.	Freq.
ft/sec	*m/s*	*c/s*	*c/s*	*c/s*	*c/s*	*c/s*
		Mode 1				
0	0	11·5	11·8	11·7	11·8	11·6
40	12·19	11·5	11·8	11·8	11·8	11·6
60	18·29	11·5	11·9	11·8	11·8	11·6
80	24·38	11·6	11·9	–	11·8	11·6
100	30·48	–	11·9	11·8	11·8	–
120	36·58	–	12·0	–	11·8	–
		Mode 2				
0	0	21·8	22·0	22·0	21·9	22·0
40	12·19	22·1	22·3	22·3	22·3	22·1
60	18·29	22·2	22·4	22·4	22·4	22·2
80	24·38	22·4	22·5	22·6	22·5	22·5
100	30·48	–	22·7	22·7	22·6	–
120	36·58	–	22·9	22·7	22·8	–
		Mode 3				
0	0	26·5	26·6	26·8	26·6	26·7
40	12·19	26·8	26·9	27·1	27·0	27·0
60	18·29	27·2	27·2	27·3	27·3	27·5
80	24·38	27·8	27·6	27·3	27·6	28·3
100	30·48	–	28·0	27·6	28·2	–
120	36·58	–	28·6	27·8	29·0	–
		Mode 4				
0	0	41·6	42·2	42·1	42·4	42·0
40	12·19	41·6	42·3	42·1	42·4	42·1
60	18·29	41·6	42·3	42·0	42·3	42·0
80	24·38	41·5	42·1	41·7	42·2	42·1
100	30·48	–	41·9	41·6	42·1	–
120	36·58	–	41·6	41·2	42·1	–

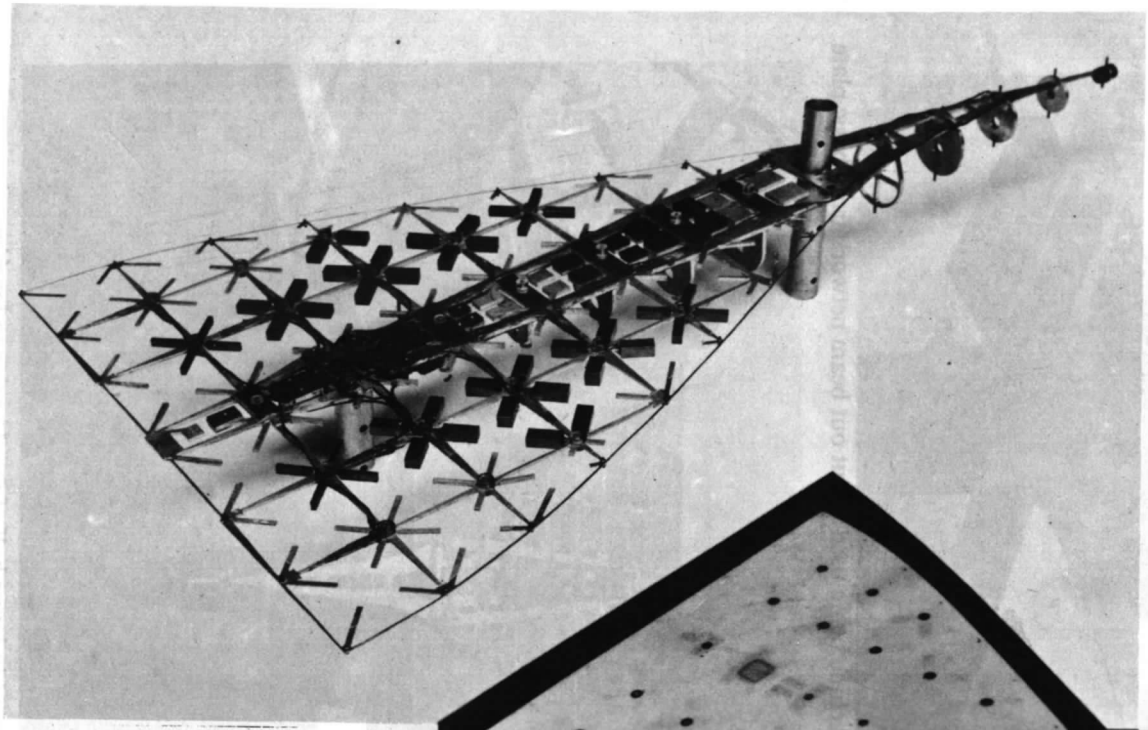

FIG. 1a. Model skeleton showing supports points, attached weights and strain gauges.

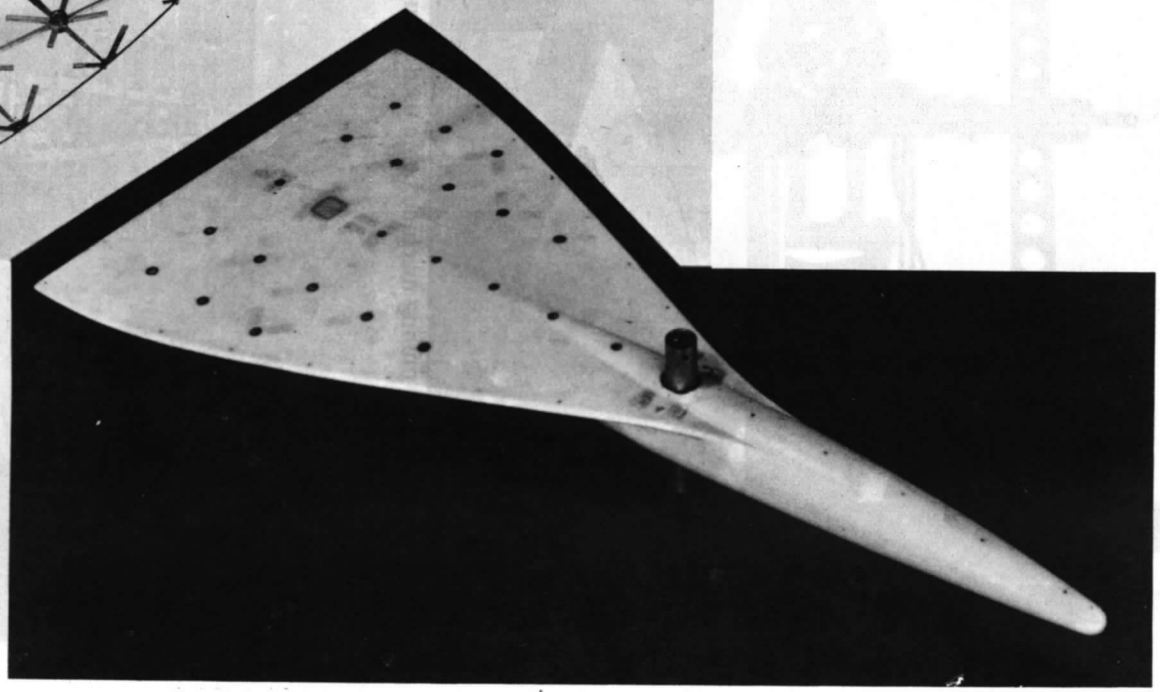

FIG. 1b. The foamed model.

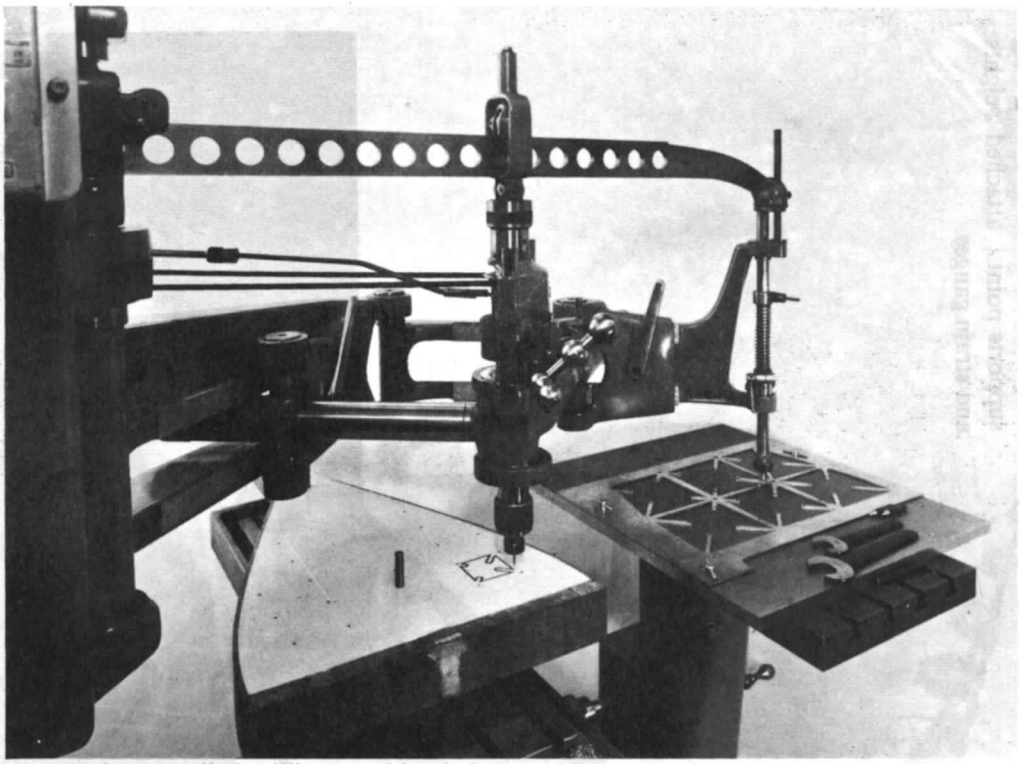

Pantograph controlled milling machine being used to cut out beam network from basic plate.

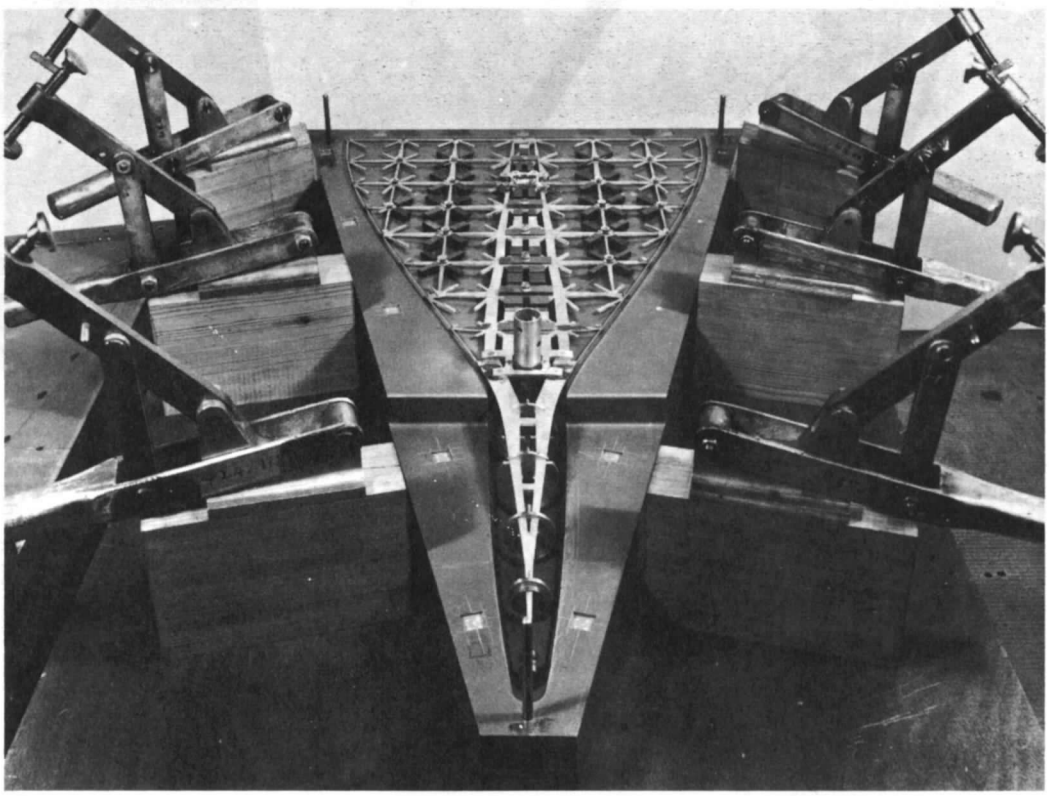

Model skeleton positioned in lower half of mould prior to foaming.

FIG. 2. Steps in manufacture of model.

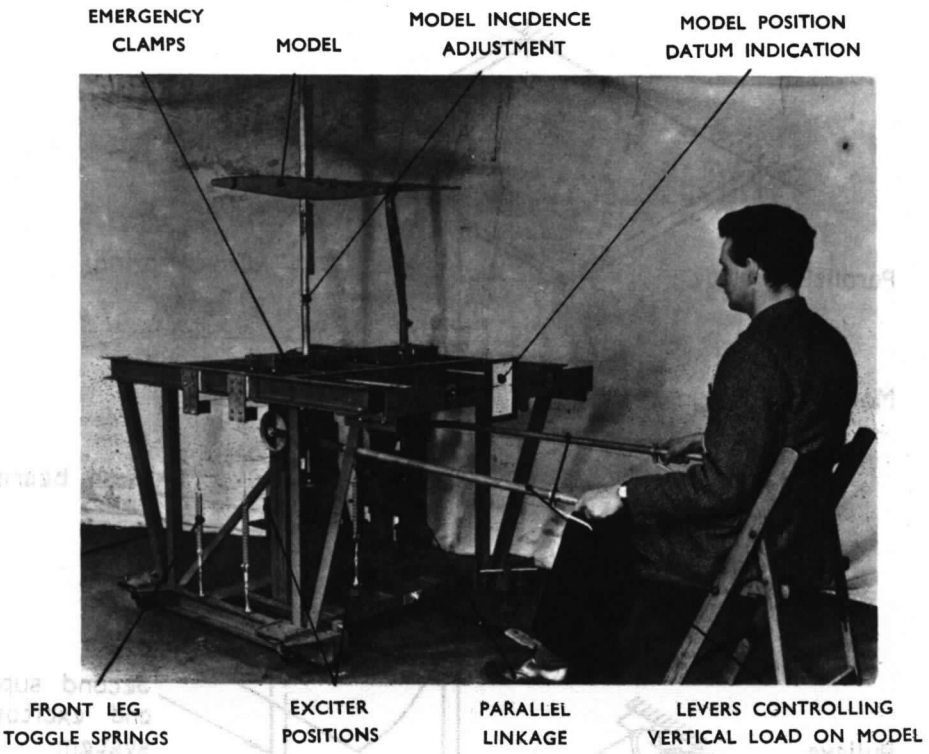

FIG. 3. Low stiffness support rig.

FIG. 4. Model installed in wind tunnel.

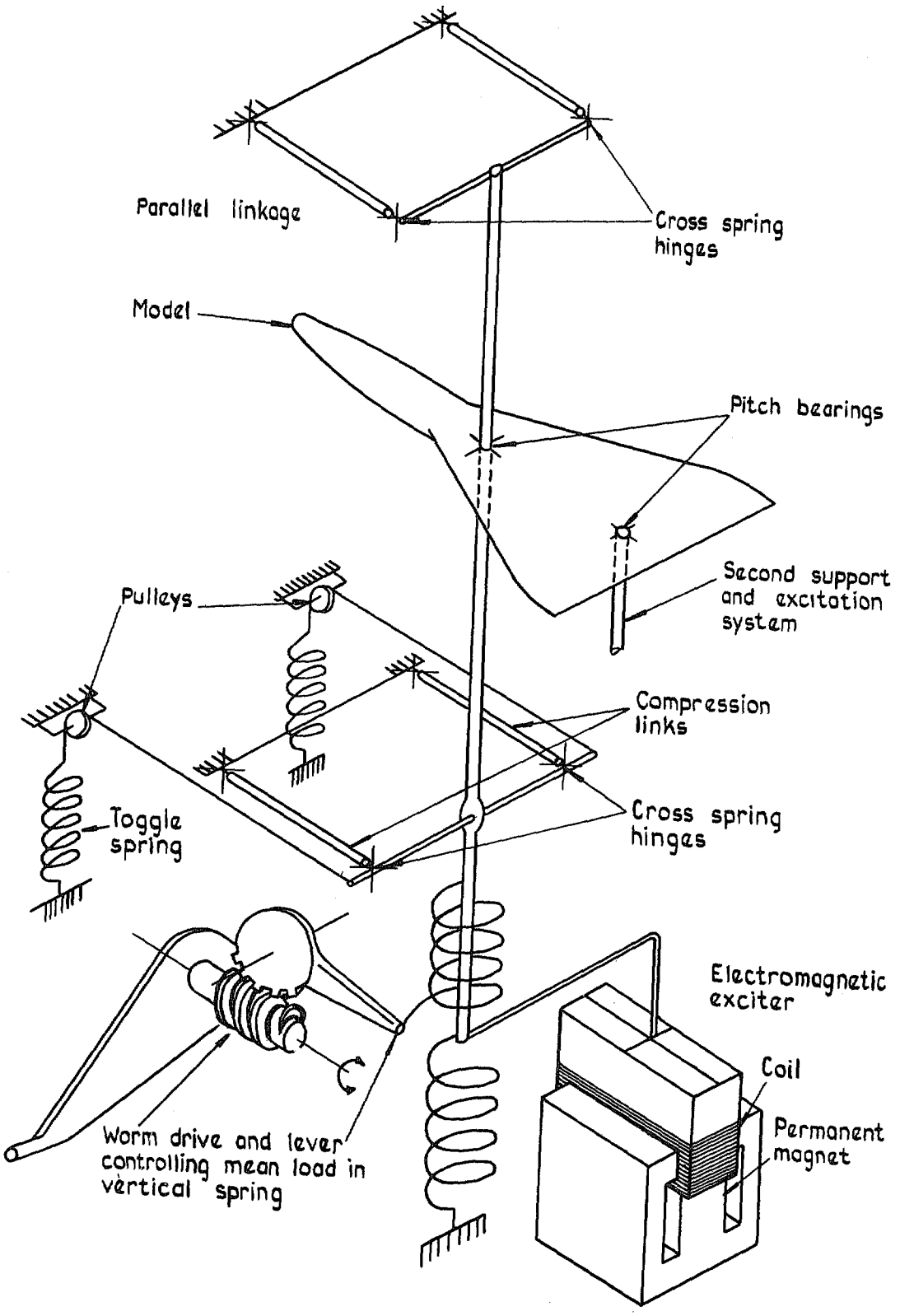

FIG. 5. Schematic diagram of model support.

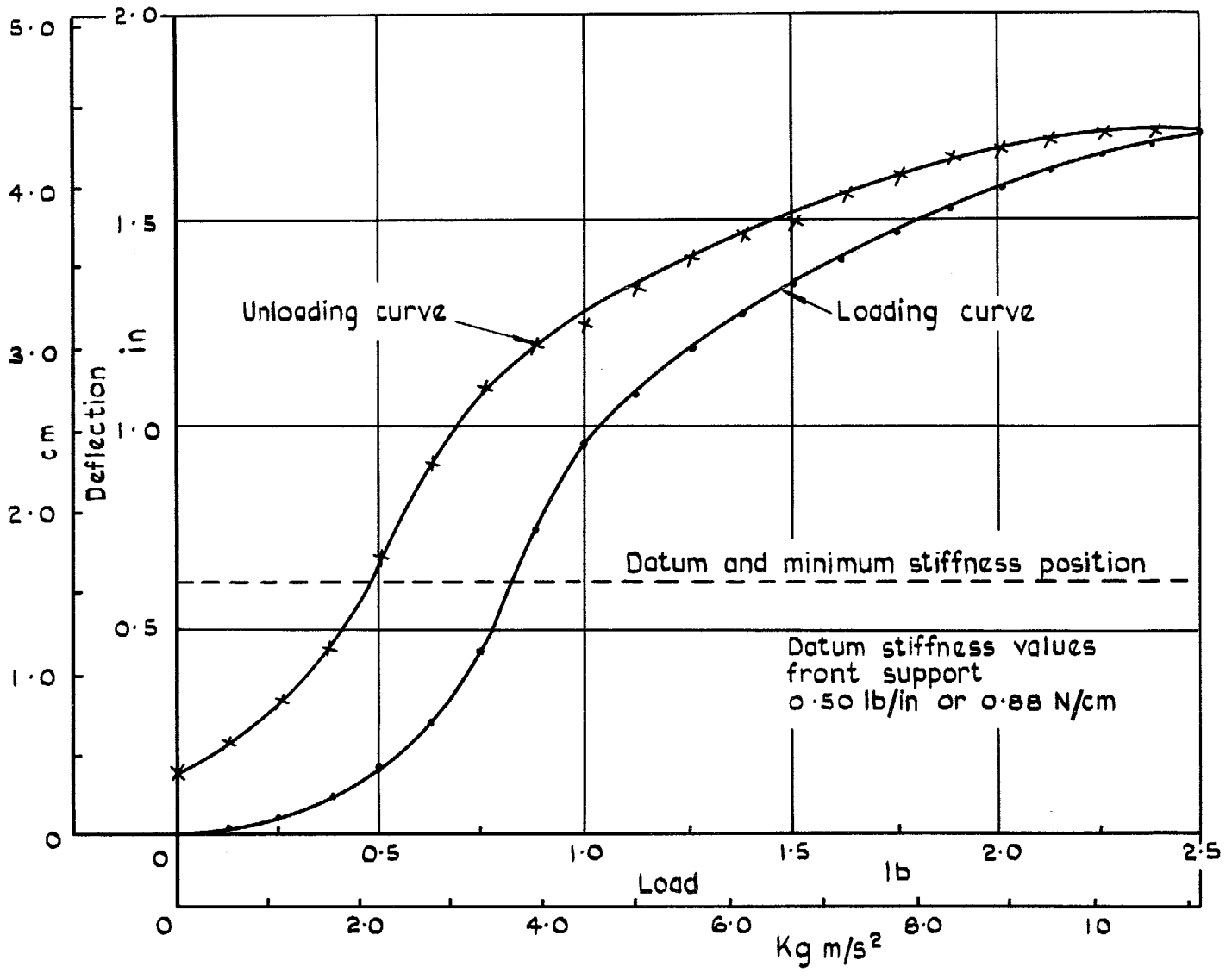

FIG. 6. Stiffness characteristics of model support rig (front leg).

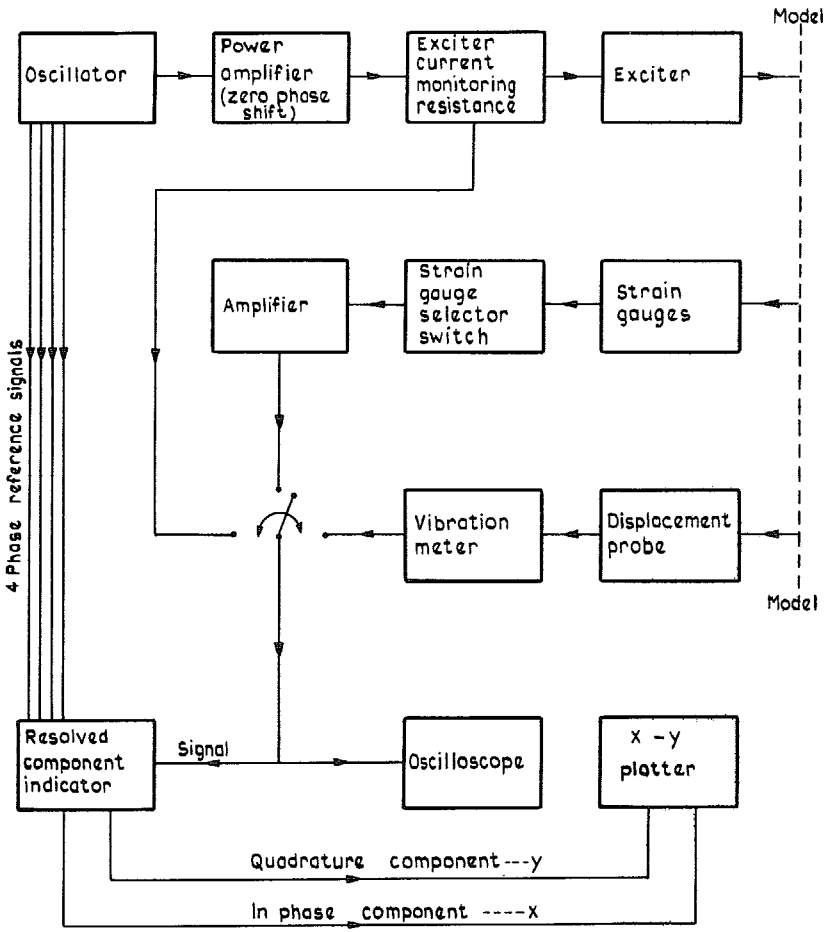

FIG. 7. Apparatus for excitation and response measurement of slender wing model.

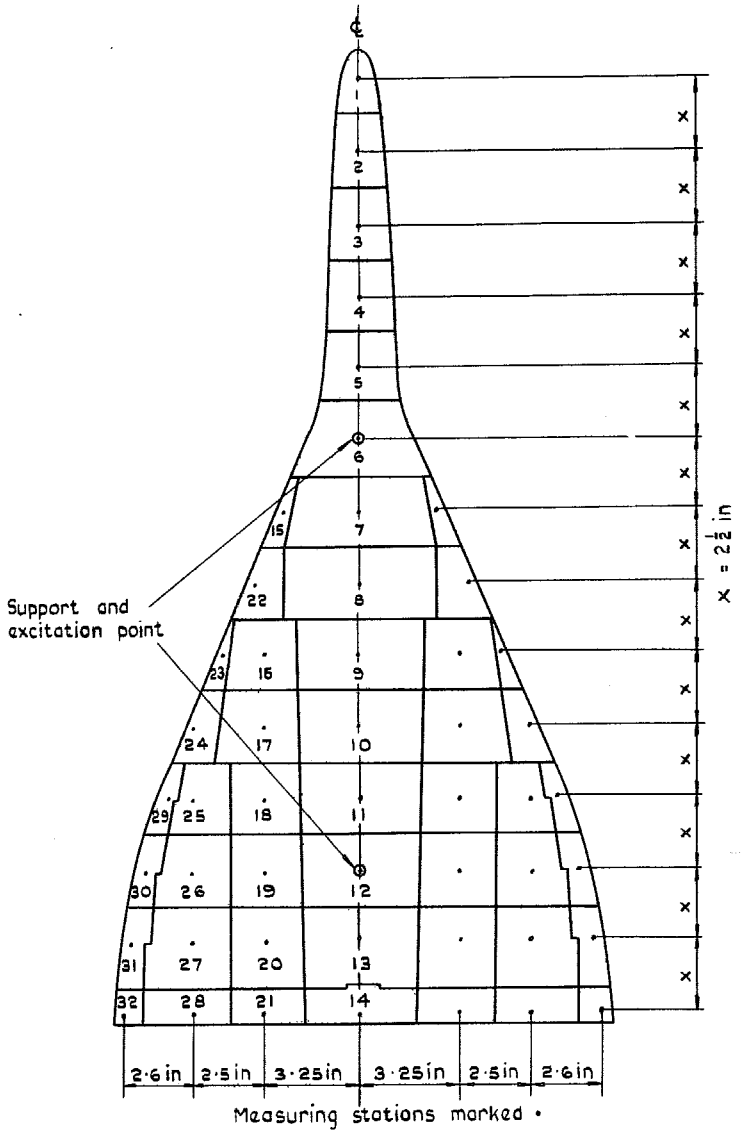

FIG. 8. Model displacement measuring stations with mass division boundaries.

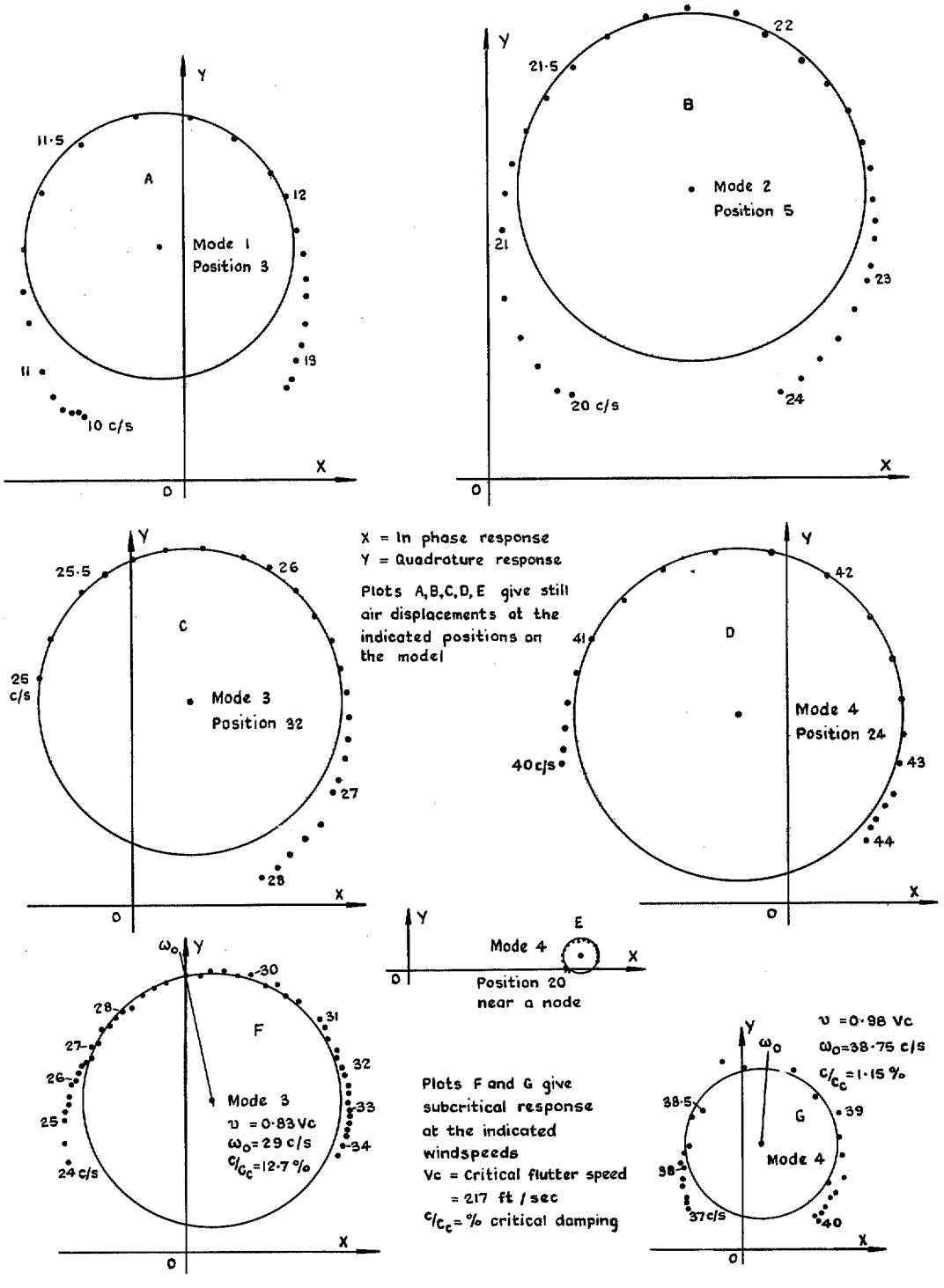

FIG. 9. Typical response plots obtained in the tests.

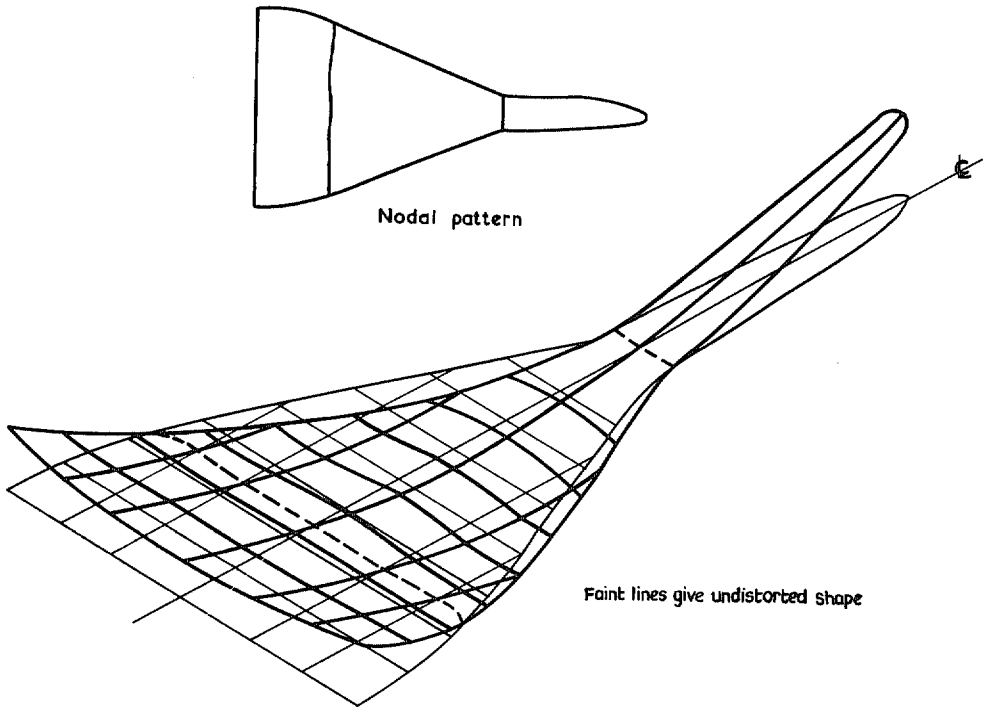

FIG. 10. 1st Deformation mode. Frequency 12·1 c/s.

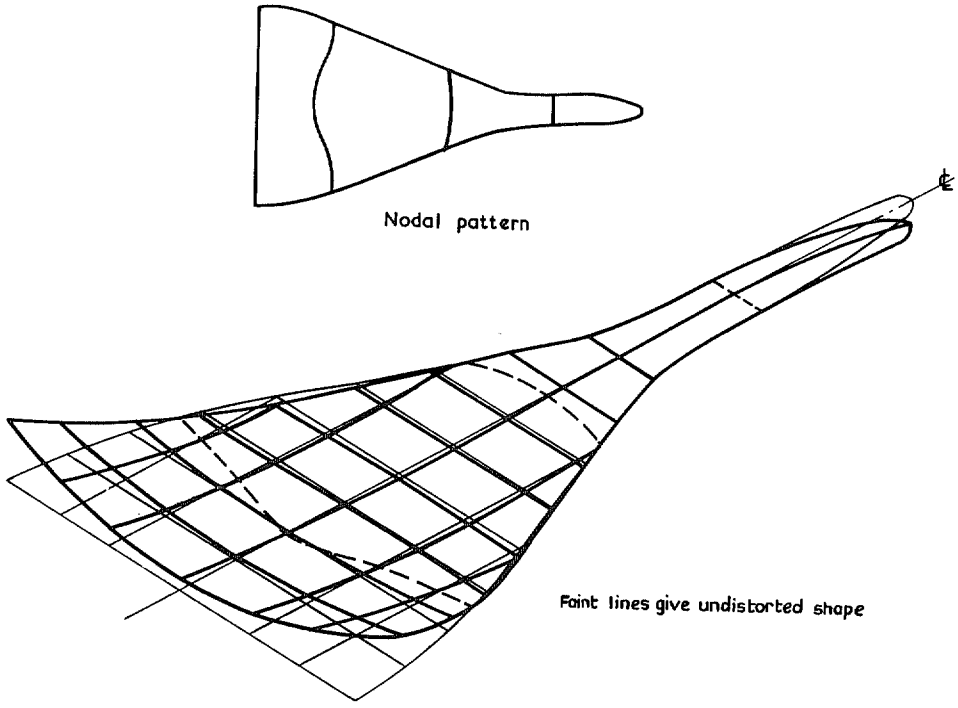

FIG. 11. 2nd Deformation mode. Frequency 22·3 c/s.

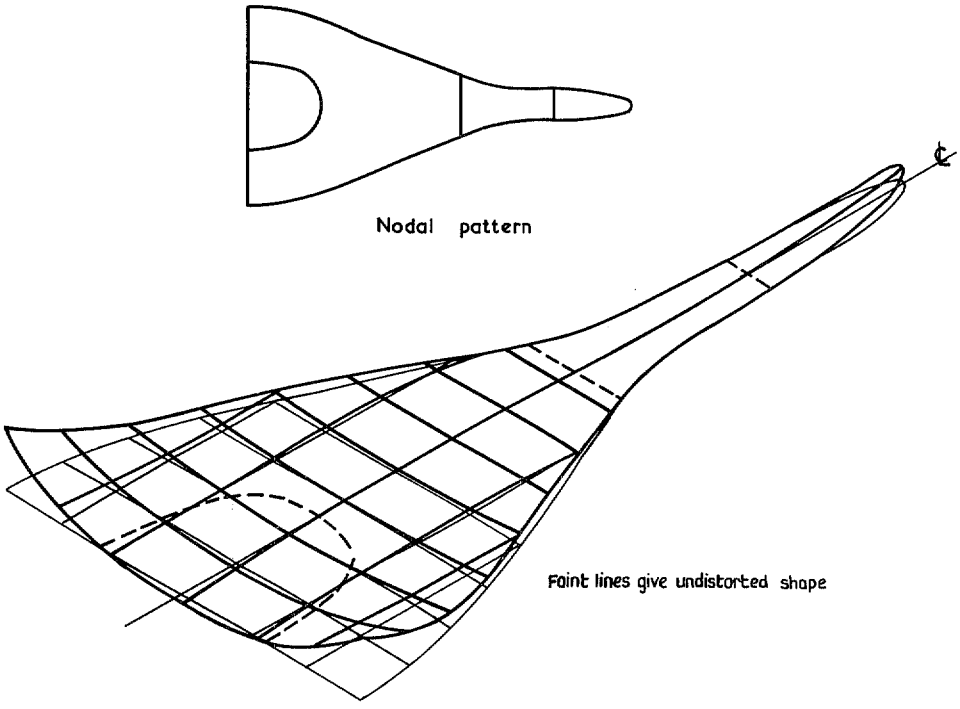

FIG. 12. 3rd Deformation mode. Frequency 26·5 c/s.

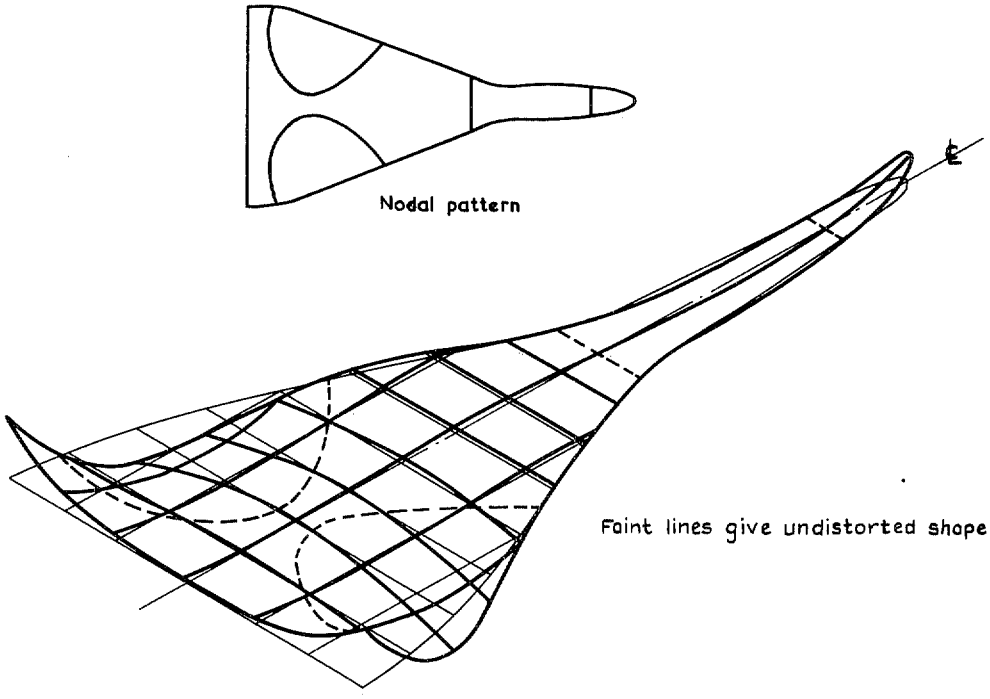

FIG. 13. 4th Deformation mode. Frequency 42·3 c/s.

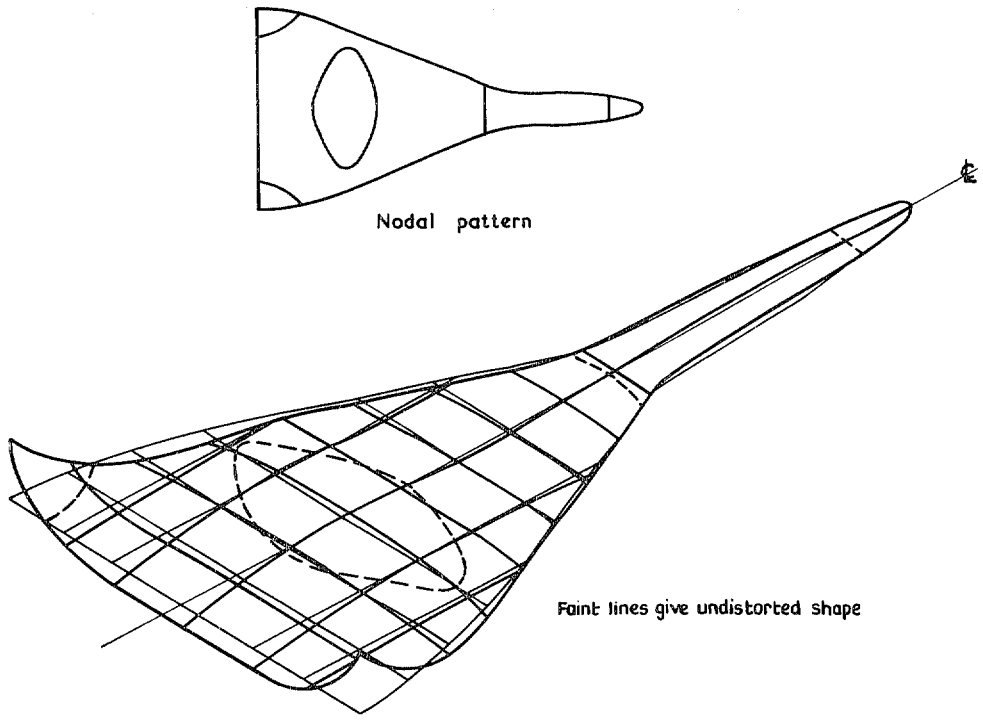

FIG. 14. 5th Deformation mode. Frequency 52·0 c/s.

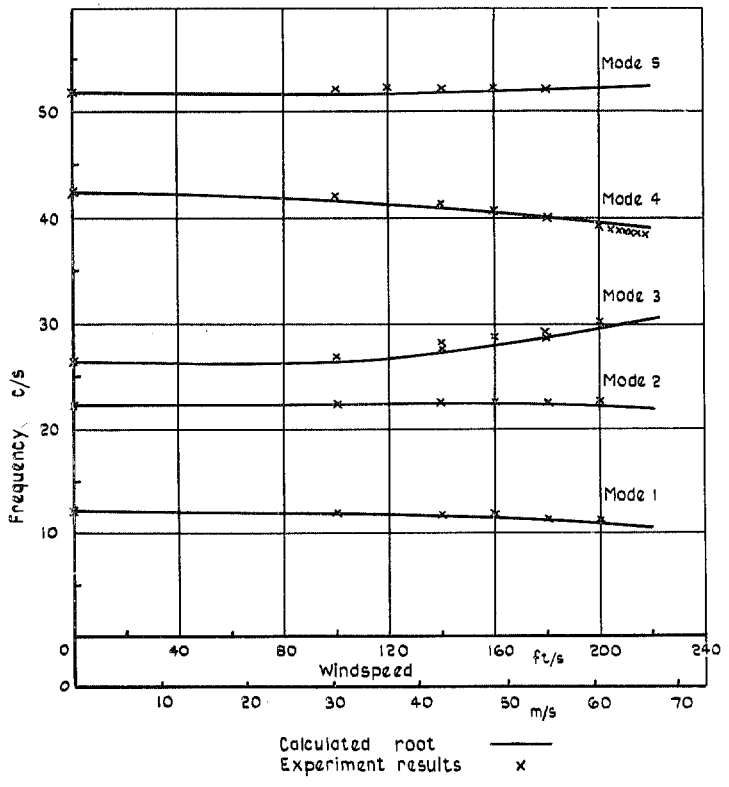

FIG. 15. Variation of model frequency with windspeed for modes 1 to 5.

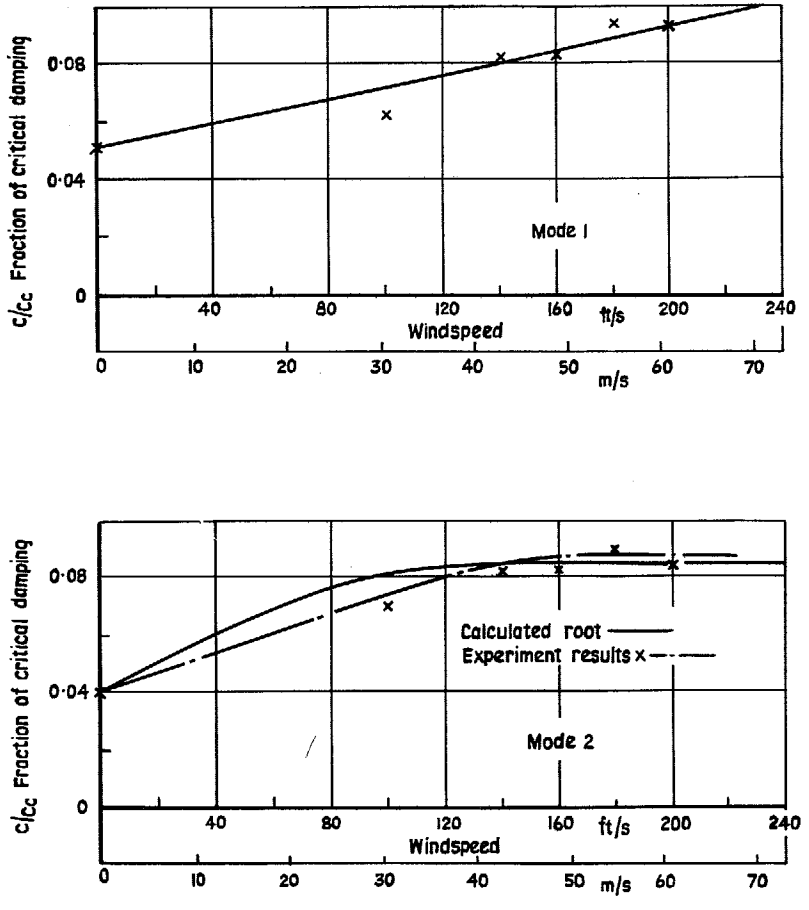

FIG. 16. Variation of model damping with windspeed for modes 1 and 2.

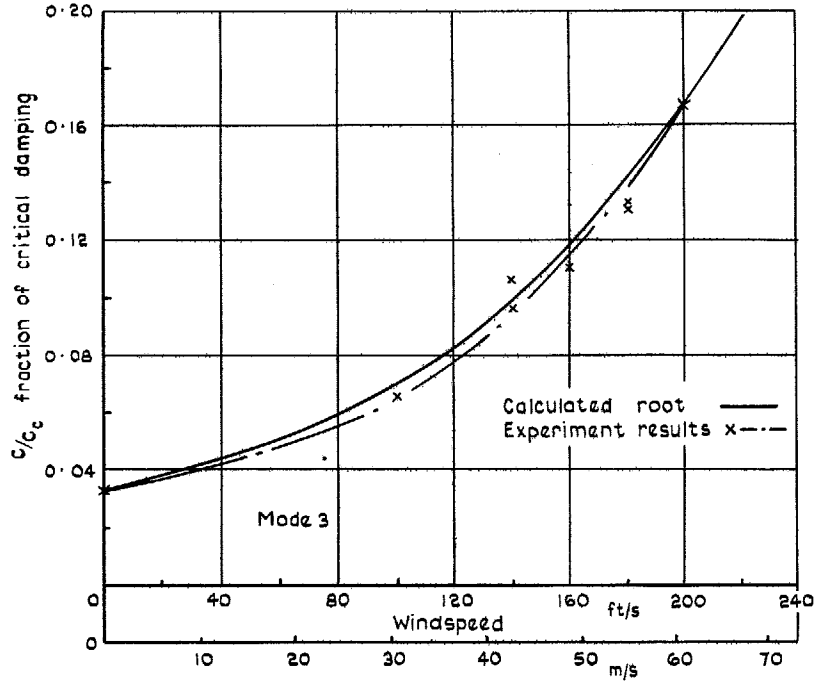

FIG. 17. Variation of model damping with windspeed for mode 3.

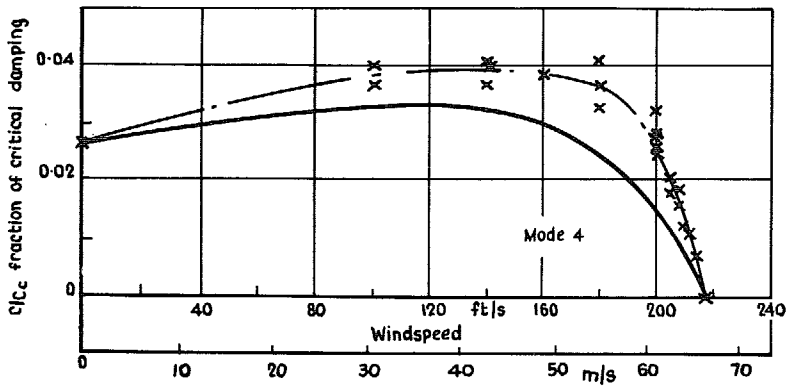

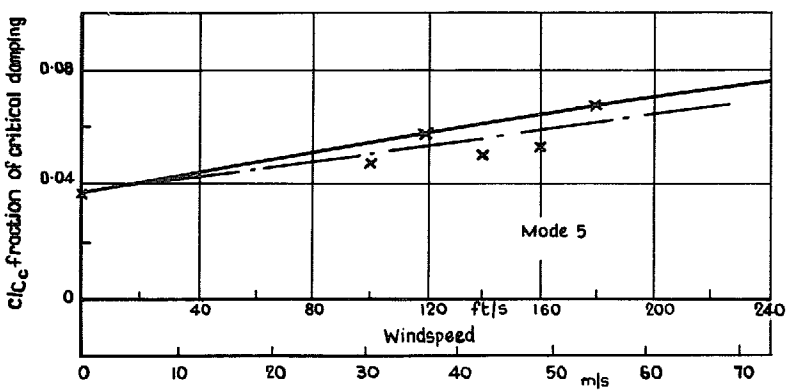

FIG. 18. Variation of model damping with windspeed for modes 4 and 5.

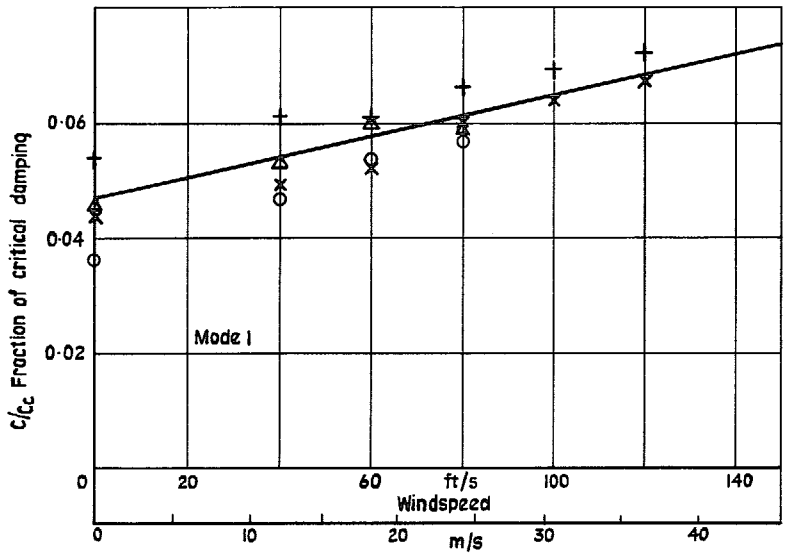

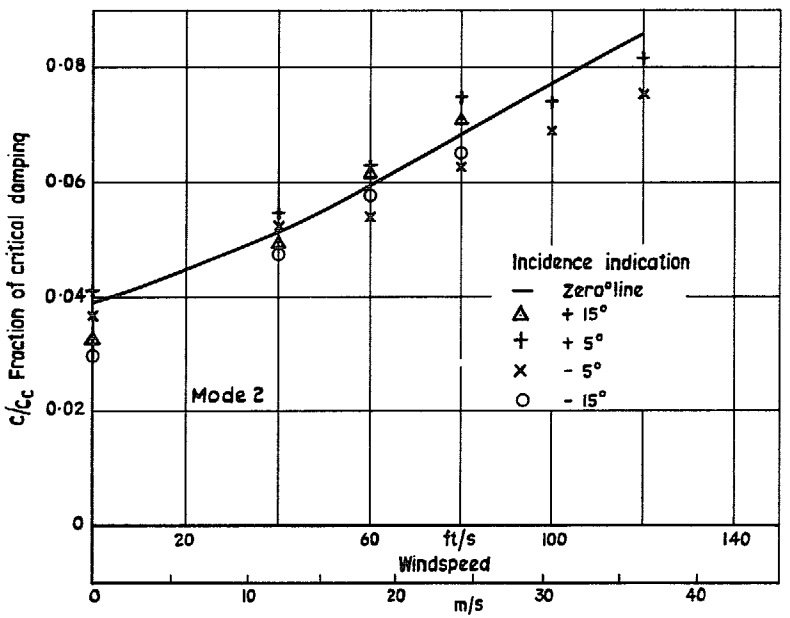

FIG. 19. The effect of incidence on the damping of modes 1 and 2.

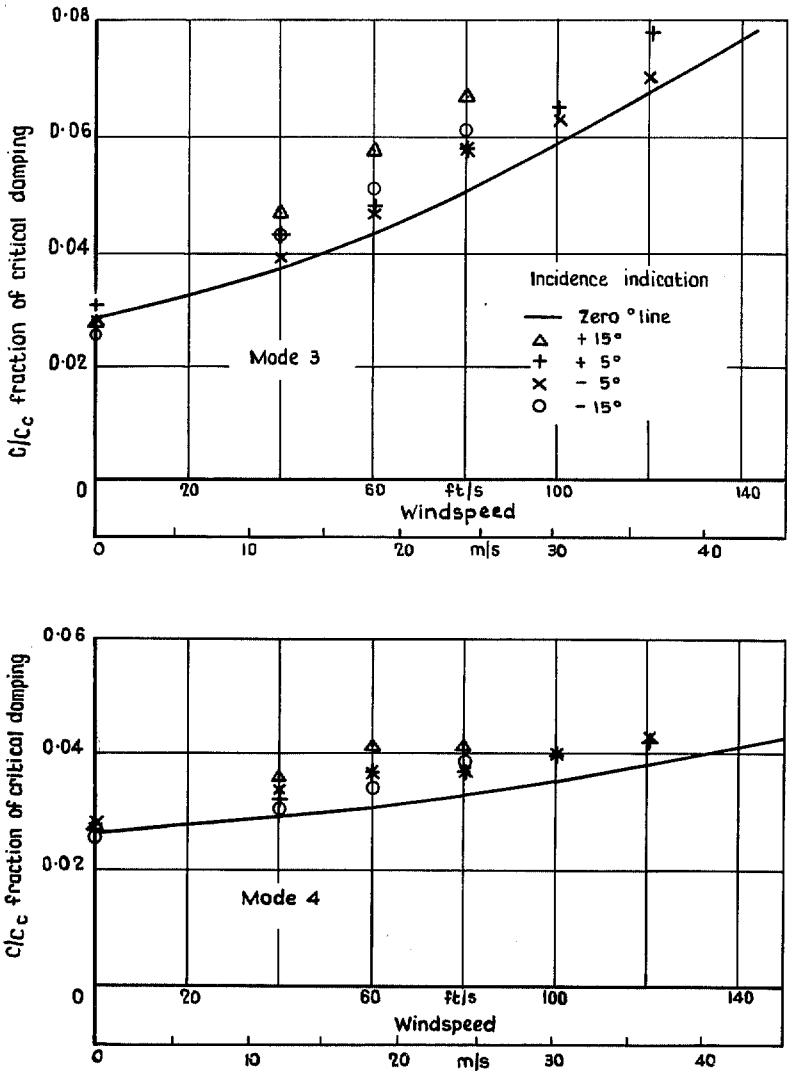

FIG. 20. The effect of incidence on the damping of modes 3 and 4.

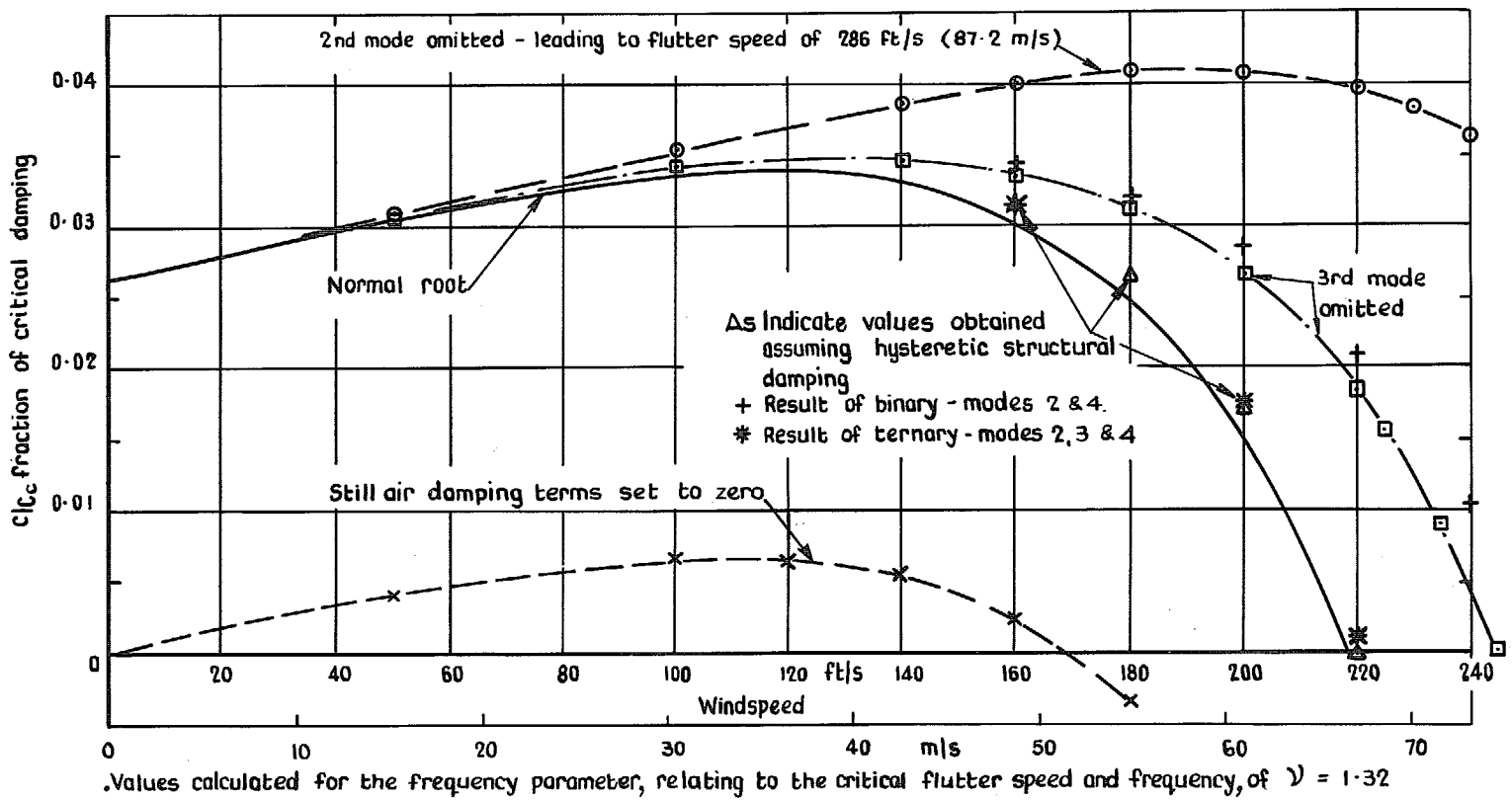

FIG. 21. Effect on the root of the 4th mode of various modifications to the coefficients of the flutter equations.

Dd.135646 K.5.

Printed in Wales for Her Majesty's Stationery Office by Allens Printers (Wales) Limited

Published by
HER MAJESTY'S STATIONERY OFFICE

To be purchased from
49 High Holborn, London W.C.1
13A Castle Street, Edinburgh 2
109 St. Mary Street, Cardiff CF1 1JW
Brazennose Street, Manchester M60 8AS
50 Fairfax Street, Bristol BS1 3DE
258 Broad Street, Birmingham 1
7 Linenhall Street, Belfast BT2 8AY
or through any bookseller

R. & M. No. 3572
S.O. Code No. 23-3572